PRAMANA
— journal of
physics

Vol. 75, No. 2
August 2010
pp. 171–183

The canonical and grand canonical models for nuclear multifragmentation

G CHAUDHURI[1,*] and S DAS GUPTA[2]
[1]Variable Energy Cyclotron Centre, 1/AF, Bidhan Nagar, Kolkata 700 064, India
[2]Physics Department, McGill University, Montréal, Canada H3A 2T8
[*]Corresponding author. E-mail: gargi@veccal.ernet.in

Abstract. Many observables seen in intermediate energy heavy-ion collisions can be explained on the basis of statistical equilibrium. Calculations based on statistical equilibrium can be implemented in microcanonical ensemble, canonical ensemble or grand canonical ensemble. This paper deals with calculations with canonical and grand canonical ensembles. A recursive relation developed recently allows calculations with arbitrary precision for many nuclear problems. Calculations are done to study the nature of phase transition in nuclear matter.

Keywords. Nuclear multifragmentation; phase transition; isoscaling.

PACS Nos 25.70.Mn; 25.70.Pq

1. Introduction

The statistical model of nuclear disassembly in heavy-ion collisions is quite successful. Here one assumes that depending upon the original beam energy, the disintegrating system may undergo an initial compression and then begins to decompress. As the density of the system decreases, higher density regions will develop into composites. As this collection of nucleons begins to move outward, rearrangements, mass transfers, nucleon coalescence and most physics will happen until the density decreases so much that the mean free paths for such processes become larger than the dimension of the system. Interactions between the different composites in the rarefied situation can be neglected (except for the long-range Coulomb interaction) and one can do a statistical equilibrium calculation to obtain the yields of composites at a volume called the freeze-out volume. The central assumption of this work is that equilibrium statistical mechanics can be used to describe the hot fluid of nucleons. Even the well-prepared experimental measurement of an energetic nucleus–nucleus collision represents the average of a very large number of initial states. In addition to this large number of different initial states, a large number of nucleon–nucleon collisions occurs within each nucleus–nucleus collision. Together this means that for many experimental observables, almost all the relevant phase space can be opened up and can be described by the statistical ensembles. The partitioning into available channels can be solved in the canonical ensemble

where the number of particles in the nuclear system is finite (as would be in experiments). In some experiments, the number of particles can fluctuate around a mean value. In such a case a sum of several canonical calculations could be appropriate. Even when the number of particles is fixed, one can hope to replace a canonical model calculation by a grand canonical model calculation where the particle number fluctuates but the average number can be constrained to a given value. Usually the grand canonical model is more easily solved and hence it is more commonly used although in the case of nuclear physics the use of the canonical ensemble would be more appropriate. Apart from the ease of calculation, there is another reason why the grand canonical model is very useful. Known properties of nuclear interactions predict that if nuclear systems were arbitrarily large (consider a fictitious system where the Coulomb interaction is switched off) disassembly of nuclear systems would show features of liquid–gas phase transition [1]. Since the grand canonical ensemble is expected to become accurate for large systems, this would seem to be a suitable framework to describe bulk properties.

The basic assumption that the break up of a hot system can be calculated by the laws of equilibrium thermodynamics has been implemented in different versions according to degrees of sophistication and detail. Thus, we have the statistical multifragmentation model (SMM) of Copenhagen [2], the microcanonical models of Gross [3] and Randrup and Koonin [4]. An easily implementable canonical ensemble model was later introduced [5]. The advantage of this soluble statistical model is that it is simple to implement and one can eliminate the computationally intensive Monte Carlo procedures by using the recursive technique of Chase and Mekjian [6]. The details of the model and many applications can be found in [7].

It has been customary to pay a great deal of attention to the production cross-sections of intermediate mass fragments and light charged particles. Here we study the properties of the largest fragment that emerges in multifragmentation and compare with experimental data. These properties are not easy to study but the canonical model allows for such computation. As part of a drive toward understanding the production mechanisms of rare isotopes, we also do calculations for the production cross-sections of neutron-rich isotopes from projectile fragmentation using the canonical thermodynamical model. Some of the cross-sections are very small and serve as stringent tests of the model. Isoscaling is a robust feature to emerge in recent experimental intermediate energy heavy-ion collisions. We have done isoscaling calculations with the canonical as well as the grand canonical models and discuss the possible deviations from isoscaling. We show that the canonical model can explain the results while the grand canonical model fails for heavier composites. We have also used the grand canonical model for nuclear matter calculations in order to study the signatures of liquid–gas phase transition in the model.

In §2 we describe the canonical and the grand canonical models briefly and in §3 we present the results calculated with the models. Summary is presented in the last section.

2. The canonical and the grand canonical models

The canonical thermodynamic model is based on the analytic evaluation of the canonical partition function for the fragmenting source with A nucleons and Z

protons (neutron number $N = A - Z$) at a given temperature T. The canonical partition function is given by

$$Q_{N_0,Z_0} = \sum \prod \frac{\omega_{I,J}^{n_{I,J}}}{n_{I,J}!}. \tag{1}$$

Here the sum is over all possible channels of break-up (the number of such channels is enormous) which satisfy $N_0 = \sum I \times n_{I,J}$ and $Z_0 = \sum J \times n_{I,J}$; $\omega_{I,J}$ is the partition function of one composite with neutron number I and proton number J respectively and $n_{I,J}$ is the number of this composite in the given channel. The one-body partition function $\omega_{I,J}$ is a product of two parts: one arising from the translational motion of the composite and another from the intrinsic partition function of the composite:

$$\omega_{I,J} = \frac{V_f}{h^3}(2\pi mT)^{3/2}A^{3/2} \times z_{I,J}(\text{int}). \tag{2}$$

Here $A = I + J$ is the mass number of the composite and V_f is the volume available for translational motion; V_f will be less than V, the volume to which the system has expanded at break up. We use $V_f = V - V_0$, where V_0 (excluded volume) is the normal volume of nucleus with Z_0 protons and N_0 neutrons. This is meant to take care of hard-sphere interactions between different particles. This is an approximate answer and the correct answer is multiplicity-dependent. In this calculation we have used a fairly typical value $V = 6V_0$. The assumption that the interaction between different composites is only reflected through an excluded volume and that this excluded volume is independent of multiplicity is an idealization which will fail for a non-dilute system. The approximation of non-interacting composites in a volume gets worse as the volume decreases. We therefore restrict this model to volumes $V_f \geq 2V_0$.

The probability of a given channel $P(\vec{n}_{I,J}) \equiv P(n_{0,1}, n_{1,0}, n_{1,1}, \ldots, n_{I,J}, \ldots)$ is given by

$$P(\vec{n}_{I,J}) = \frac{1}{Q_{N_0,Z_0}} \prod \frac{\omega_{I,J}^{n_{I,J}}}{n_{I,J}!}. \tag{3}$$

The average number of composites with I neutrons and J protons is seen easily from the above equation to be

$$\langle n_{I,J} \rangle = \omega_{I,J} \frac{Q_{N_0-I,Z_0-J}}{Q_{N_0,Z_0}}. \tag{4}$$

The constraints $N_0 = \sum I \times n_{I,J}$ and $Z_0 = \sum J \times n_{I,J}$ can be used to obtain different looking but equivalent recursion relations for partition functions. For example

$$Q_{N_0,Z_0} = \frac{1}{N_0} \sum_{I,J} I\omega_{I,J} Q_{N_0-I,Z_0-J}. \tag{5}$$

These recursion relations allow one to calculate Q_{N_0,Z_0} very easily.

We list now the properties of the composites used in this work. The proton and the neutron are fundamental building blocks. Thus, $z_{1,0}(\text{int}) = z_{0,1}(\text{int}) = 2$ where 2 takes care of the spin degeneracy. For deuteron, triton, ^{3}He and ^{4}He we use $z_{I,J}(\text{int}) = (2s_{I,J}+1)\exp(-\beta E_{I,J}(\text{gr}))$ where $\beta = 1/T$, $E_{I,J}(\text{gr})$ is the ground state energy of the composite and $(2s_{I,J}+1)$ is the experimental spin degeneracy of the ground state. Excited states for these very low mass nuclei are not included. For mass number $A = 5$ and more we use the liquid-drop formula. For nuclei in isolation, this reads ($A = I + J$) as

$$z_{I,J}(\text{int}) = \exp\frac{1}{T}\left[W_0 A - \sigma(T)A^{2/3} - \kappa\frac{J^2}{A^{1/3}} - C_s\frac{(I-J)^2}{A} + \frac{T^2 A}{\epsilon_0}\right]. \tag{6}$$

The derivation of this equation is given in several places [2,7] and so we will not repeat the arguments here. The expression includes the volume energy, the temperature-dependent surface energy, the Coulomb energy and the symmetry energy. The term T^2A/ϵ_0 represents contribution from excited states since the composites are at a non-zero temperature. The long-range Coulomb interactions between different composites can be included in an approximation called the Wigner–Seitz approximation. We incorporate this following the scheme set up in [2]. For I, J (the proton and the neutron numbers) we include a ridge along the line of stability. The liquid-drop formula above also gives neutron and proton drip lines and results include all nuclei within the boundaries.

We now briefly review the grand canonical model. For finite systems such as considered here, it is inferior to the canonical model but is easier to implement. If the numbers of neutrons and protons in the dissociating system are N_0 and Z_0 respectively, the ensemble contains not only these but many others but the average value can be constrained to be N_0 and Z_0. The chemical potentials μ_n and μ_p serve to fix the average numbers. If the neutron chemical potential is μ_n and the proton chemical potential is μ_p, then statistical equilibrium implies that the chemical potential of a composite with N neutrons and Z protons is $\mu_\text{n}N + \mu_\text{p}Z$. The following are the relevant equations for us. The average number of composites with N neutrons and Z protons is

$$\langle n_{N,Z}\rangle = \mathrm{e}^{\beta\mu_\text{n}N+\beta\mu_\text{p}Z}\omega_{N,Z}. \tag{7}$$

These are the two equations which determine μ_n and μ_p.

$$N_0 = \sum N\mathrm{e}^{\beta\mu_\text{n}N+\beta\mu_\text{p}Z}\omega_{N,Z} \tag{8}$$

$$Z_0 = \sum Z\mathrm{e}^{\beta\mu_\text{n}N+\beta\mu_\text{p}Z}\omega_{N,Z}. \tag{9}$$

The sum here is over all nuclei within drip lines whose (N, Z) do not exceed (N_0, Z_0) since there cannot be a composite whose N, Z exceed those of the system from which it emerges.

We want to point out the following feature of the grand canonical model. In all $\omega_{N,Z}$'s in the sum in the above two equations, there is one common value for V_f

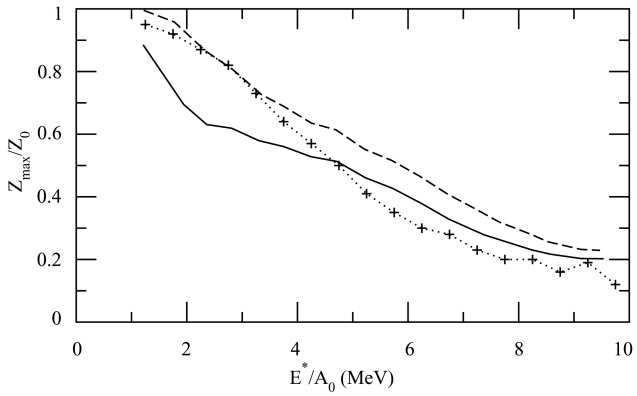

Figure 1. Experimental points (from figure 1f of [8]) are joined by a dotted line to guide the eye. The calculations are exploratory: these are done for a fixed freeze-out density (solid line for $\rho/\rho_0 = 0.25$ and dashed line for $\rho/\rho_0 = 0.39$). The calculations shown here include the composites of set 1 (refer §3.1).

(see eq. (2)). We really solve for N_0/V_f and Z_0/V_f. The values of $\mu_{\rm n}$ or $\mu_{\rm p}$ will not change if we, say, double N_0, Z_0 and V_f simultaneously provided the number of terms in the sum is unaltered. We then might as well say that when we are solving the grand canonical equation we are really solving for an infinite system (because we know that fluctuations will become unimportant) but this infinite system can break up into only certain kinds of species as are included in the above two equations. Which composites are included in the sum is an important physical ingredient in the model but intensive quantities like β and μ depend not on N_0, Z_0 but on N_0/V_f and Z_0/V_f. To apply the grand canonical model to finite systems after solving for μ's, we plug in the value of V_f that would be appropriate for the system N_0, Z_0. If the system which we are investigating is small, experimental data may show substantial deviations from the grand canonical model as we will verify later.

3. Results

3.1 *Size of the largest cluster from the decay of excited projectile-like fragment*

In the EOS experiment, part of the projectile (Au, La and Kr) is sheared off by the ^{12}C target. We will compare our calculations with the Au + C data. The size of the excited PLF which decays depends upon the impact parameter which also determines the amount of excitation energy per nucleon in the excited PLF. In figures 1b and 1c of [8] the size of the excited PLF (the size and charge are denoted by A_0 and Z_0) is plotted as a function of excitation energy E^* per nucleon. This aspect of the experiment depends upon dynamics and is outside the scope of a thermodynamic model. However, given E^* and A_0, Z_0, this excited PLF will expand and break up into many pieces and this is calculable in a canonical thermodynamic model. In figure 1 (data taken from figure 1f of [8]) we have plotted $Z_{\rm max}/Z_0$ as

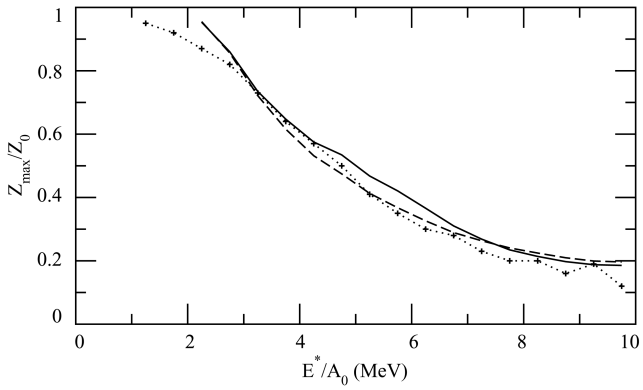

Figure 2. It is expected that the freeze-out density will decrease with excitation energy in this energy range. The calculations here use a parametrization $\rho/\rho_0 = a + b\exp(-c(E^*/A_0))$ where $a = 0.17$, $b = 0.83$ and $c = 0.417$ MeV^{-1}. The solid line uses set 1 and the dashed line uses set 2. Experimental data are joined by a dotted line.

a function of E^* per nucleon where $Z_{\max}$ is the average maximum charge carried by a composite. The data are shown as stars joined by a dotted curve. The other curves are exploratory calculations. Our fit to experimental data is given in figure 2. We now explain how the calculations are done.

For a given value of A_0, Z_0, the experiment provides the value of E^*. The beginning of a canonical thermodynamic model besides A_0, Z_0, are a temperature and a freeze-out density ρ/ρ_0 (freeze-out density in unit of normal nuclear density $\rho_0 = 0.16$ fm^{-3}) which will then provide all the observables including E^*. For a fixed E^* the canonical model employs a fixed ρ/ρ_0. However, in the EOS experiment, E^* varies over a wide range (from less than 2 MeV per nucleon where the validity of the thermodynamic model as used here can be questioned to 10 MeV per nucleon where the thermodynamic model is expected to work well) and hence we should expect that ρ/ρ_0 will also need to vary in this interval. In general, the freeze-out density will decrease as M/A_0 ($M =$ multiplicity, $A_0 =$ mass number of the dissociating system) increases, reaching some asymptotic value for large multiplicity. In SMM [2] the freeze-out density varies in each channel, decreasing as the multiplicity increases (this makes Monte–Carlo simulation mandatory). In the canonical model, at a given temperature, the freeze-out density is kept fixed irrespective of channels. Thus the freeze-out density can be dependent only on the average multiplicity. For I, J (the proton and the neutron numbers) we include a ridge along the line of stability. We have used two sets to test the sensitivity of the results to the width of of the ridge. We call these set 1 and set 2. In set 1 for each a between 5 and 40, five isotopes are included (cases for $a = 4$ and lower were already mentioned before); For $a > 40$, seven isotopes are included for each a. In set 2, five isotopes are used for a between 5 and 9, seven isotopes are used for a between 10 and 40 and nine isotopes for $a > 40$. The results are quite similar in most cases. It should be pointed out that enlarging the width of the ridge does not necessarily imply a better calculation as one may begin to overcount the phase space.

Figure 1 compares the data if in the calculation the freeze-out volume is kept fixed at $\rho/\rho_0 = 0.25$ (a typical canonical model value) or at 0.39 (this is an often quoted value in the model used in [8,9]). The value 0.39 is clearly better at lower values of E^* but leaves too large a residue at higher E^* whereas the value 0.25 is better at the higher end of E^* but is an underestimation at the lower end of E^*. The data undoubtedly point to the need of a variable ρ/ρ_0 if the whole spectrum of E^* is to be covered. In figure 1, for brevity we show results with set 1. Figure 2 compares data with our calculation where we use a variable ρ/ρ_0. We have used a parametrization $\rho/\rho_0 = a + b\exp(-c(E^*/A_0))$ where $a = 0.17$, $b = 0.83$ and $c = 0.417$ MeV^{-1}. No optimization of the fit was tried but the values are suitable for the low and high limits of E^*. Our values of ρ/ρ_0 are also very similar to those quoted in table 2 of [10] where a different model was used.

In the canonical model calculation normally the inputs are the freeze-out density and temperature. Here we use the freeze-out density and E^*. Given this density and E^* we find the temperature which would give back the E^* we started with. We then calculate $Z_{\max}$. Calculations for $A_{\max}$ were also done and the fits are similar.

3.2 *Cross-sections of neutron-rich nuclei from projectile fragmentation*

Fragmentation cross-sections of many neutron-rich isotopes have recently been measured from the ^{48}Ca and ^{64}Ni beams at 140 MeV per nucleon on ^{9}Be and ^{181}Ta targets [11]. Copper isotope cross-sections have been measured in projectile fragmentation of ^{86}Kr at 64 MeV per nucleon. A remarkable feature is the correlation between the measured fragment cross-section and the average binding energy (figure 1). This observation has prompted attempts of parametrization of the cross-sections. One very successful parametrization is

$$\sigma = C\exp(A^{-1}(B - \varepsilon_{\text{pair}})/\tau). \tag{10}$$

Here B is the binding energy of the nucleus with mass number A, $\varepsilon_{\text{pair}} = \kappa\varepsilon A^{-3/4}$ and κ is 1 for even–even nuclei, 0 for odd–even nuclei and -1 for odd–odd nuclei. The pairing term smooths the straggling seen in the data when logarithms of cross-sections are plotted against B/A for even–even and odd nuclei (or odd–even and odd–odd nuclei). Theoretical basis for the simple appearance of B/A or the pairing term correction is not transparent.

Here we do calculations for the production cross-sections of copper isotopes from projectile fragmentation of ^{86}Kr using the canonical thermodynamic model. Some of these cross-sections are very small and they serve as very stringent tests of the model. The model has been extensively applied for production cross-sections of other particles which are more numerous [7] and agreements are good. The basic physics of the model is the same as in many other models of intermediate energy heavy-ion collisions but SMM or the microcanonical simulations are totally impractical for calculations of very small cross-sections as they rely on Monte–Carlo simulations. The canonical model gives closed expressions and calculations can be made as accurate as desired.

We will consider the production of copper isotopes from the statistical break up of $^{86}_{36}$Kr. We denote the average number (multiplicity) of $_{29}$Cu$_n$ by $\langle n_{29,n}\rangle$. Then

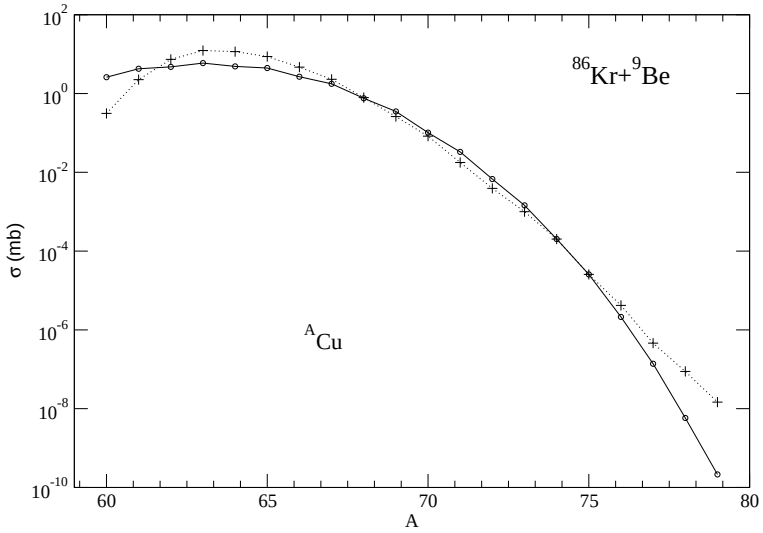

Figure 3. Experimental cross-sections for copper isotopes (circles) compared with theoretical results (crosses). A dotted line is drawn through the experimental data and a solid line through the calculated values. The temperature used is 9.5 MeV.

the cross-section will be $\sigma(29, n) = C\langle n_{29,n}\rangle$ where C is a constant not calculable from the thermodynamic model. It depends upon dynamics which is outside the scope of the model. The source sizes adopted for the calculation are zeroth order guesses. It could be sometimes smaller or greater depending on the diffusion from the target. For Cu nucleus whose production cross-section is sought in this work, we use the experimental binding energies tabulated in [12] but we also include the term T^2a/ϵ_0 for contribution from excited states.

In figure 3 we show results of our calculations (crosses) for the production of copper isotopes. There are basically two parameters: an overall normalization factor (chosen in the figure to give the correct value of cross-section for ^{75}Cu) and the temperature (taken here to be 9.5 MeV which is within the range of temperatures expected for this reaction). The data here span more than eight decades and the calculation, except for the tails, does very well. The straggling between cross-section values for odd–odd and odd copper isotopes is highlighted in figure 4. In the same figure we show that for both data and calculation the straggling disappears if the cross-section is plotted against $\langle B\rangle - \varepsilon_{\text{pair}}$ rather than against just $\langle B\rangle$ (see also [13]). We find it gratifying that the model is able to reproduce such fine details.

3.3 *Isoscaling and deviation from isoscaling*

For central collisions of Sn on Sn (^{112}Sn + ^{112}Sn, ^{124}Sn + ^{112}Sn and ^{124}Sn + ^{124}Sn) a well-known result is that the ratio of isotope yields from two different reactions, 1

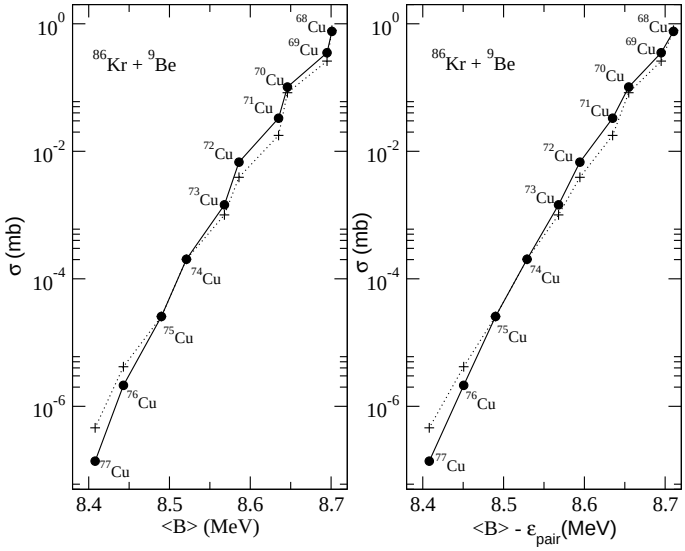

Figure 4. Straggling of data between odd–odd and odd–even cases (closed circles) when plotted against the average binding energy $\langle B\rangle = B/A$. Similar scatter is seen in theoretical calculation (crosses). On the right panel, the cross-sections are plotted against $\langle B\rangle - \varepsilon_{\rm pair}$ (see eq. (10)). The value of ε used here is 30 MeV. This decreases the straggling significantly both for data and theory.

and 2, $R_{21}(N,Z) = Y_2(N,Z)/Y_1(N,Z)$ exhibits an exponential relationship which is a function of the isotope neutron number N and proton number Z [13–15]:

$$R_{21}(N,Z) = Y_2(N,Z)/Y_1(N,Z) = C\exp(\alpha N + \beta Z). \tag{11}$$

This is called isoscaling which is a robust feature to emerge in recent experimental intermediate energy heavy-ion collisions. We now discuss isoscaling and possible deviations from it. It is a well-known fact that isoscaling works very well when N/N_0 and Z/Z_0 are small (≤ 0.35) and many experimental data fall in this range [13–15]. If we now extend these observations to larger composites, deviations are to be expected. In figure 5 we compare some experimental data with a canonical calculation. Experimental details can be found in [11]. In the experiment, reaction 1 is ^{58}Ni on ^{9}Be and reaction 2 is ^{64}Ni on ^{9}Be. For the canonical calculation, for reaction 1 the dissociating system is taken to be $^{58}\mathrm{Ni} + {}^{9}\mathrm{Be}$ ($N_0 = 35, Z_0 = 32$) and for reaction 2 the dissociating system is taken to be $^{64}\mathrm{Ni} + {}^{9}\mathrm{Be}$ ($N_0 = 41, Z_0 = 32$). All composites between drip lines are included with the highest values of N, Z terminating at N_0, Z_0. The results reproduce the experimental data reasonably well. The deviations from isoscaling for the heavier composites (as seen in the data) also emerge from the canonical model calculation (as seen in figure 5). In the canonical model, the ratio R_{21} is given by

$$R_{21} = C\frac{Q_{N_0-N,Z_0-Z}(2)}{Q_{N_0,Z_0}(2)} \Big/ \frac{Q_{N_0-N,Z_0-Z}(1)}{Q_{N_0,Z_0}(1)}. \tag{12}$$

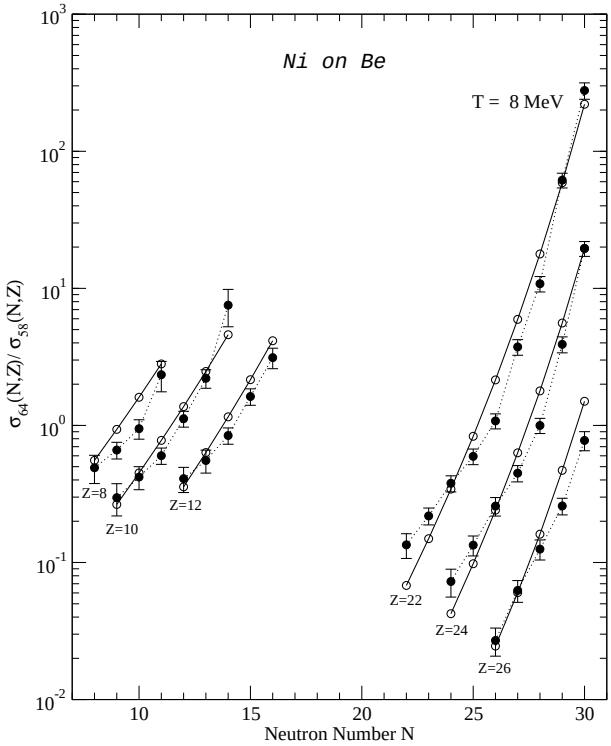

Figure 5. Ratio of cross-sections of producing the nucleus (N, Z) where reaction 1 is ^{58}Ni on ^{9}Be and reaction 2 is ^{64}Ni on ^{9}Be, both at 140 MeV/n beam energy. Experimental data with error bars are compared with theoretical results from canonical ensemble (open circles). Dotted lines are drawn through experimental points and solid lines through calculated points.

This formula is not transparent at all but reproduces isoscaling for smaller composites and the deviations from isoscaling for the heavier ones. The grand canonical model on the other hand always predicts isoscaling. The slopes of $\ln R_{21}$ as a function of N for fixed Z (a) will never deviate from a straight line and (b) for different fixed Z's the slopes will not change. In the experiments, this is not the case and the slopes for the heavier composites deviate from straight lines. From the theoretical point of view, the use of grand canonical approximation for the emissions of heavier composites is not valid. The canonical calculations (figure 5) are significantly different from the grand canonical results (figure 6) and are much closer to the experimental data.

3.4 *Signatures of phase transition in the model*

We will use the grand canonical model for nuclear matter calculations and demonstrate that the multifragmentation model predicts first-order phase transition.

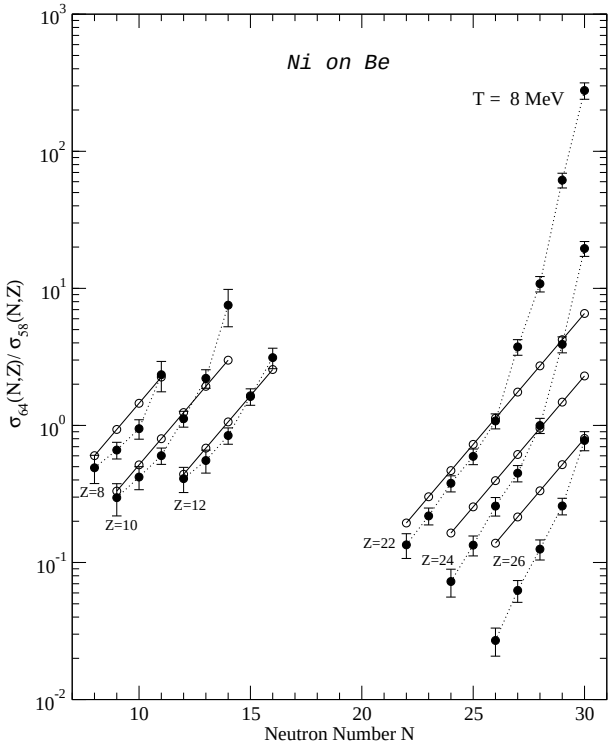

Figure 6. The same as in figure 5 except that the calculation is done in the grand canonical ensemble. Agreement with data is not good for the heavier composites.

Pressure in the model is given by $p = T(\sum n_{N,Z}/V_f) = T(\sum n_A/A_0)/(V_f/A_0) = T\rho_f(\sum n_A/A_0)$. We plot results as a function of ρ rather than ρ_f the connection being $\rho_f = \rho\rho_0/(\rho_0 - \rho)$. We have $\rho = \rho_n + \rho_p$. We need an asymmetry parameter and use N_0/Z_0 for the same. We denote the size of the largest fragment (cluster) that is formed as a result of multifragmentation by $A_{\max}$. In principle this should be ∞ but for practical calculations one needs to restrict this to a maximum value that we label as $A_{\max}$. Earlier calculations with one kind of particles showed that with $A_{\max} = 200$ features of liquid–gas phase transition are not revealed (see figure 14 in [7]) but a high value of $A_{\max}$ of 2000 produces a nearly perfect model of phase transition (elaborated in much larger detail in [16,17]).

In figure 7 we show p–ρ/ρ_0 curves for $N_0/Z_0 = 1.4$ where the values of $A_{\max}$ are 200, 400, 600, 800 and 1000. The temperature used is 6.5 MeV. For all five choices of $A_{\max}$, pressure against ρ initially rises quite sharply and then flattens out considerably. The initial stage of fast rise of pressure with density is the gas phase. Here the results do not matter whether $A_{\max}$ is 200, 400 or larger. The reason is explained in detail in [18]. The flattening which follows depends on $A_{\max}$ but above a large enough value of $A_{\max}$ it will not change. For one kind of particles this is reached around 2000 [18]. However, the choice of $A_{\max} = 600$ is good enough for at

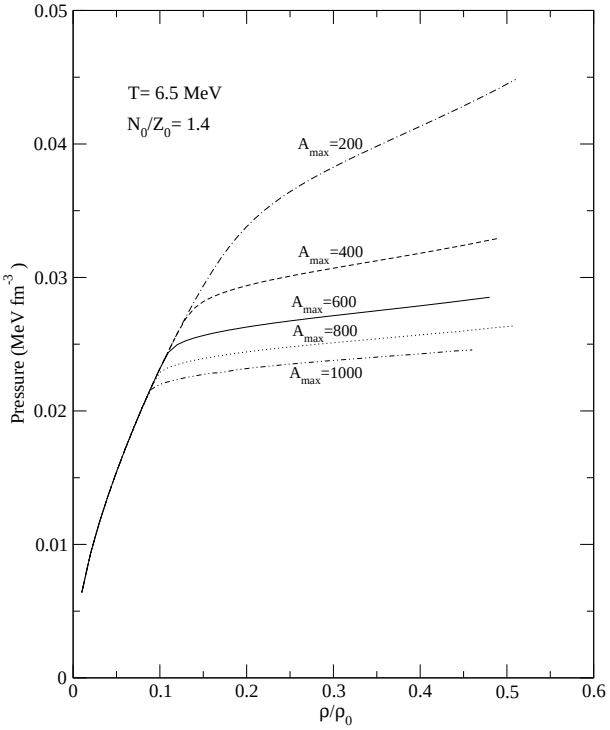

Figure 7. Pressure–density curves for $N_0/Z_0 = 1.4$ and $T = 6.5$ MeV, where the values of $A_{\max}$ used are 200, 400, 600, 800 and 1000. Note that in the region of fast rise of pressure with density results are insensitive to the value $A_{\max}$. In the high density side pressure appears to approach a constant value as a function of density as the value of $A_{\max}$ is increased.

least a semiquantitative estimate of various thermodynamic properties of nuclear matter and we will present results for this value although we did some calculations with other choices of $A_{\max}$ also. The flattening happens slightly beyond $\rho/\rho_0 = 0.1$. We show results up to $\rho/\rho_0 = 0.5$ arguing that the excluded volume correction for interactions between composites becomes worse with increasing density. The rise of pressure at small density followed by a flattening of p with increasing density is a signature of the first-order liquid–gas transition. Beyond a certain temperature, the flatness will disappear showing that there is no more phase transition in the domain $\rho/\rho_0 \leq 0.5$.

Below the density where phase transition sets in, the system is in pure gas phase. At phase transition point some liquid will be formed and the fraction of nucleons in the liquid phase will grow at the expense of the gas particles as the density increases. This can actually be followed. One also gets a functional definition of what constitutes the gas particles. Here our identification is very different from what is concluded in [17] but very similar to what is found in our earlier work with one kind of particles [16].

4. Summary

The canonical thermodynamic model is very easy to implement and yet it is very realistic. It clearly reproduces important features of the largest fragment resulting from multifragmentation. The same model gives remarkable fits to light charged particles and intermediate mass fragments. It also reproduces the salient features of production cross-sections of very neutron-rich nuclei. The model also reproduces isoscaling and the deviations from the same. We also showed that one must give up using the grand canonical ensemble for finite systems and instead use models that strictly conserve neutron and proton numbers. The multifragmentation model, so useful for fitting experimental data in intermediate energy collisions, leads naturally to a model of phase transition for nuclear matter. In a range of temperature and density, first-order transition occurs and the gas and the liquid phases can be clearly identified. This is most remarkable and the model of multifragmentation may be unique in this respect.

References

[1] S Das Gupta, A Z Mekjian and M B Tsang, *Advances in nuclear physics* (Springer Verlag, 2001), Vol 26, p. 91
[2] J P Bondorf, A S Botvina, A S Iljinov, I N Mishustin and K Sneppen, *Phys. Rep.* **257**, 133 (1995)
[3] D H Gross, *Phys. Rep.* **279**, 119 (1997)
[4] J Randrup and S E Koonin, *Nucl. Phys.* **A471**, 355c (1987)
[5] S Das Gupta and A Z Mekjian, *Phys. Rev.* **C57**, 1361 (1998)
[6] K C Chase and A Z Mekjian, *Phys. Rev.* **C52**, R2339 (1995)
[7] C B Das, S Das Gupta, W G Lynch, A Z Mekjian and M B Tsang, *Phys. Rep.* **406**, 1 (2005)
[8] J B Elliott *et al*, *Phys. Rev.* **C67**, 024609 (2003)
[9] J A Hauger *et al*, *Phys. Rev.* **C62**, 024616 (2000)
[10] J A Hauger *et al*, *Phys. Rev.* **C57**, 764 (1998)
[11] M Mocko *et al*, *Phys. Rev.* **C74**, 054612 (2006)
[12] G Audi, A H Wapstra and C Thibault, *Nucl. Phys.* **A729**, 337 (2003)
[13] M B Tsang, W A Friedman, C K Gelbke, W G Lynch, G Verde and H S Xu, *Phys. Rev. Lett.* **86**, 5023 (2001)
[14] H S Xu *et al*, *Phys. Rev. Lett.* **85**, 716 (2000)
[15] M B Tsang *et al*, *Phys. Rev.* **C64**, 054615 (2001)
[16] G Chaudhuri, S Das Gupta and M Sutton, *Phys. Rev.* **B74**, 174106 (2006)
[17] J N De and S Samaddar, *Phys. Rev.* **C76**, 044607 (2007)
[18] G Chaudhuri and S Das Gupta, *Phys. Rev.* **C76**, 014619 (2007)